Pivotal role of solid-phase interactions for the pressure-induced bi-stability of cyanide-bridged Fe_2Co_2 square complexes

Buqin Xu,[a] Yanling Li*,[a] Geoffrey Gontard,[a] Keevin Béneut,[b] Paraskevas Parisiades,[b] Maxime Deutsche,[c] and Rodrigue Lescouëzec*[a]

Supplementary information

I. FTIR and TGA spectra of 3 and 4

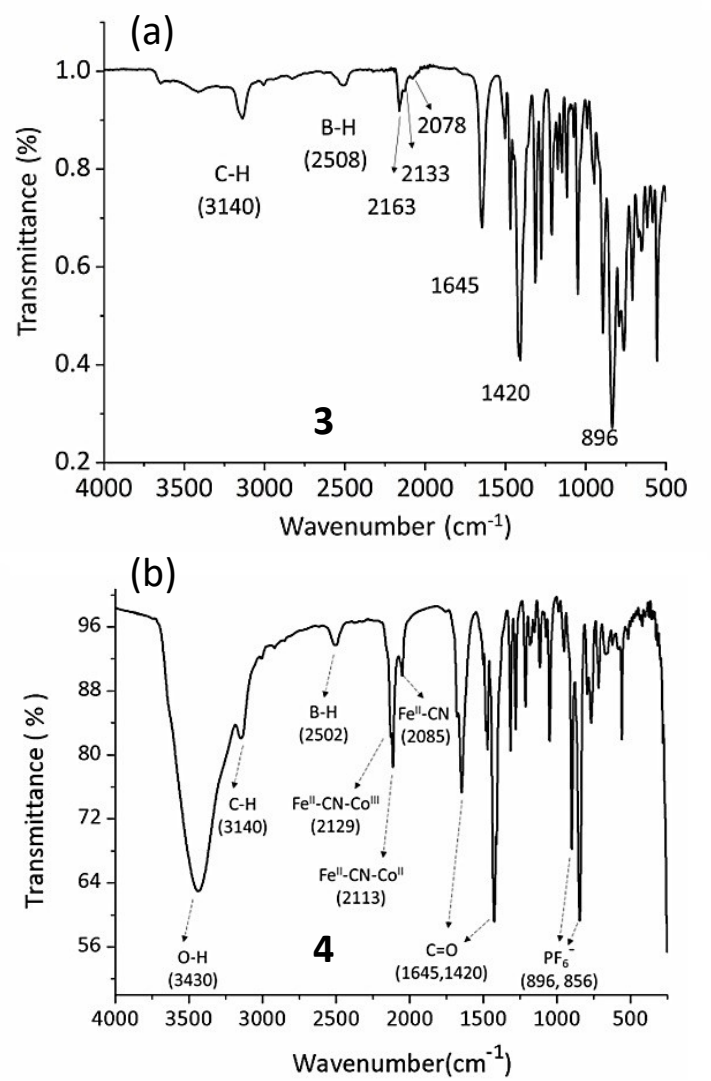

Figure S1. FTIR spectrum of compound **3** (a) and **4** (b).

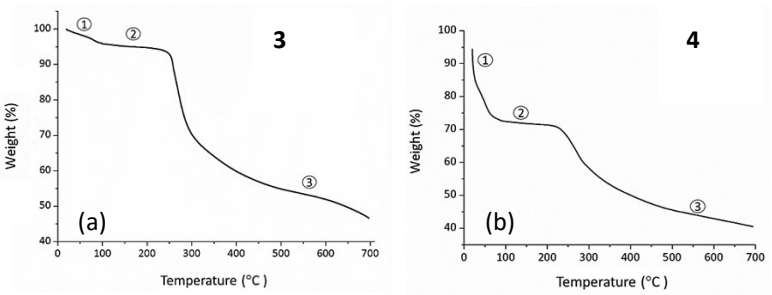

Figure S2. TGA spectrum of **3** (a) and **4** (b) under N_2 flow.

II. Structure and crystal packing of 3 and 4 at 200 K and ambient pressure

Table S1. Crystallographic data and refinement for **3** and **4**.

Compound	**3**	**4**
T (K)	200	200
Formula	$C_{68}H_{60}B_2Co_2Fe_2N_{34}O_4$ ·2PF6·2CH3OH	$C_{68}H_{60}B_2Co_2Fe_2N_{34}O_4$ ·2PF6
Mol Wt.(g/mol)	2022.70	1958.62
space group	Triclinic P-1	Triclinic P-1
a (Å)	13.773(2)	15.4654(6)
b (Å)	14.300(2)	17.5513(7)
c (Å)	14.438(2)	19.6656(8)
α (°)	114.695(3)	80.292(2)
β (°)	95.479(4)	79.298(2)
γ (°)	116.910(3)	84.572(2)
V [Å3]	2157.0(6)	5159.0(4)
Z	1	2
$\rho_{calcg/cm3}$	1.557	1.261
μ[mm-1]	0.842	5.655
Independent reflections	10707	10769
Completness	1.000	0.996
R1 [I≥2σ(I)]	0.0419	0.0619
wR2 (all data)	0.1085	0.1748
CCDC n°	2265639	2265640

Table S2. Main structural parameters of **3** and **4**.

Parameter group	**Compound**	**3**	**4**	
			Sqr a	**Sqr b**
Average M-L length (Å)	Fe-(CN)bridging	1.918 (2.5)	1.846 (8)	1.858 (7.5)
	Fe-N(Tp)	1.975 (2.7)	2.003 (5.7)	2.002 (6.7)
	Co-(NC)bridging	2.112 (2.5)	1.902 (7)	1.873 (6)
	Co-N(vbik)	2.137 (2.3)	1.912 (5.8)	1.922 (5.5)
Different Angles (°)	∑Fe	23.00	25.60	25.4
	∑Co	38.06	18.40	15.70
	∠N1C1-Fe or ∠N8C35-Fe	172.2 (3)	176.4 (7)	174.6 (6)
	∠N2C2-Fe or ∠N19C36-Fe	176.5 (3)	176.2 (6)	174.9 (6)
	∠C1N1-Co or ∠C35N18-Co	167.1 (2)	174.1 (6)	172.2 (6)
	∠C2N2-Co or ∠C36N19-Co	159.3 (2)	172.1 (6)	172.2 (2)
	Apex angle N-Co-N	93.7 (1)	92.3 (3)	92.2 (2)
	Apex angle C-Fe-C	85.6 (1)	87.6 (3)	88.3 (3)
vbik Conformat. (°)	∠Co-C=O1 or∠Co-C=O3	175.38	160.6	162.5
	∠Co-C=O2 or ∠Co-C=O4	173.97	162.9	161.0
	Dihedral angle vbik1	8.83	23.3	25.1
	Dihedral angle vbik2	11.69	24.9	28.4
Side and diagonal distances (Å)	d1[Fe···Co]	5.109	4.878	4.877
	d2[Fe···Co]	5.077	4.862	4.872
	diag[Fe···Fe]	7.470	7.037	7.058
	diag[Co···Co]	6.926	6.734	6.725

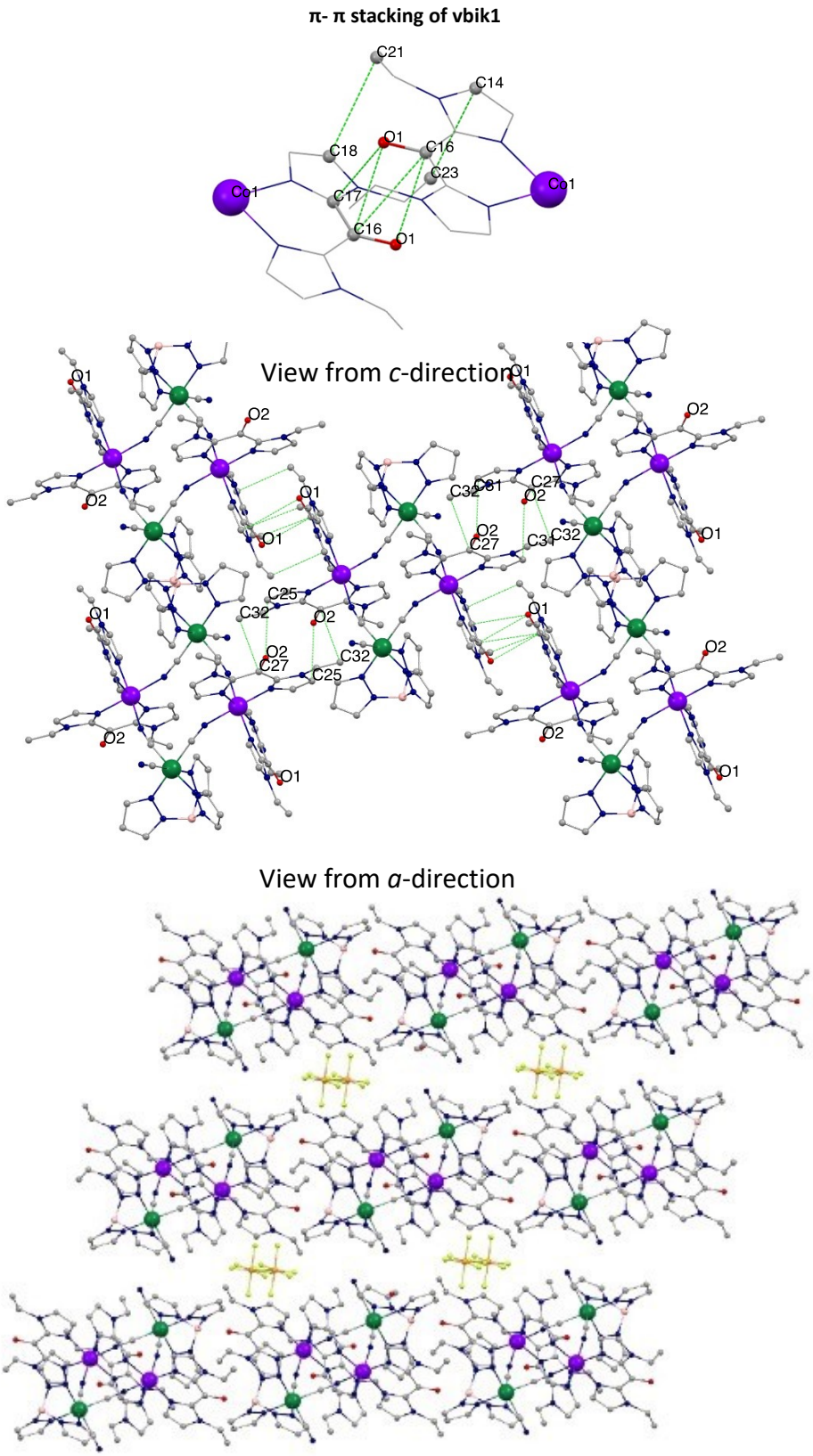

Fig S3. Crystal packing of **3**. Views from the *c*- (above) and a- (bottom) directions.

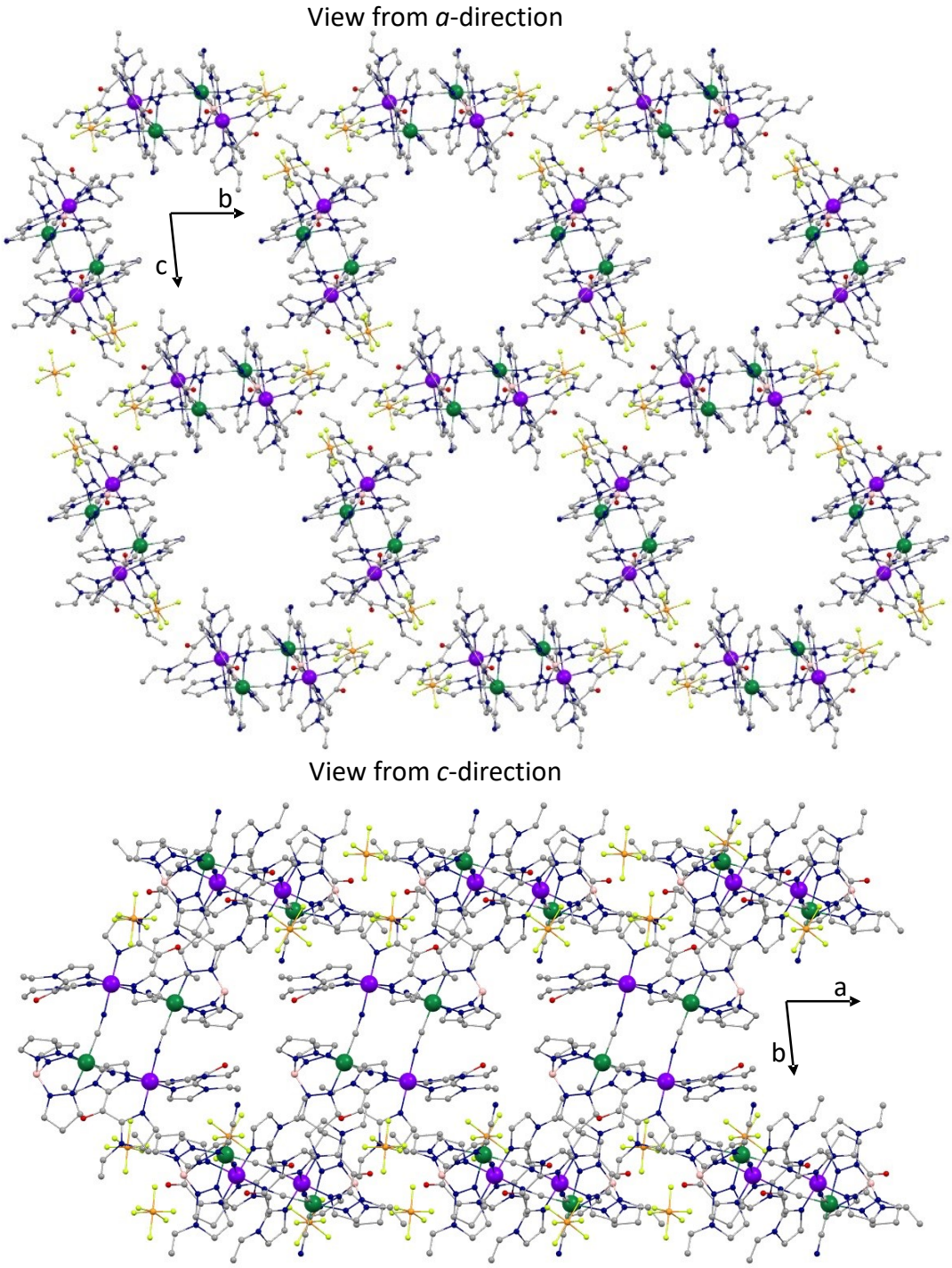

Fig S4. Crystal packing of **4**. Views from *a*-direction (top)and *c*-direction (bottom) respectively.

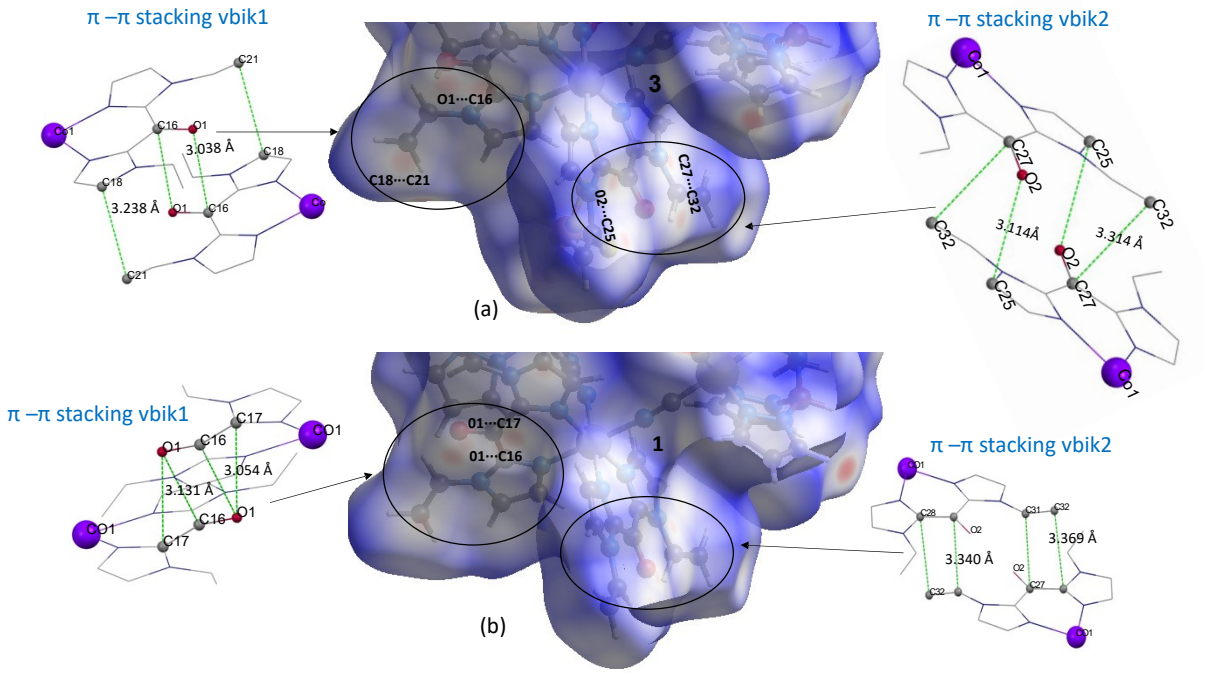

Figure S5. Hirshfeld surface (HS) analysis of vbik π-π stackings in **3** (a) and in **1** (b) at 200 K. The HS analysis was done on the structural data with H atom positions normalized by Mercury.

Table S3. Short contact distance over d_{VdW} (%) in **3** and in **1** at 200K under ambient pressure.

Contact type	Short Contact	**3**	**1**
π-π stacking	O1···C16	94.3	98.2
vbik1	O1···C17	98.6	92.8
vbik1- vbik2 (of the same square)	O1···H24	92.0	92.1
π-π stacking	O2···C25	96.7	
vbik2	C27···C32	97.5	
	C27···C31		95.5
Important H···F*	Contact number	5	4
contact of anion	av.contact distance	85.4	86.3

* Short contacts giving red spots on Hirshfeld surface (d_{VdW} = 2.67 Å).

Comparison of tree main types of intermolecular interactions of **3** and **1** at ambient pressure.

1. For vbik1 stacking, the distance between C=O groups arranged parallelly is 3.038 Å in 3 (d/d_{VdW} = 94.3%) and 3.131 Å in 1 (d/d_{VdW} = 97.2%), with d_{VdW} =3.22 Å for O···C short contact. The C=O pair interaction should have higher strength in **3**.

2. For vbik2 stacking, both C27···C32 and 02···C25 short contacts in **3** are visible as red spots on its HS. This is not the case for the C27···C31 and C28···C32 short contacts in **1**. It is obvious that the vbik2 stacking is stronger in **3**.

3. The H···F short contacts are more numerous in **3** than in **1** and the average H···F distance is shorter in **3** (table S4).

IV. ETCST properties of 1 and 3 under various under pressure

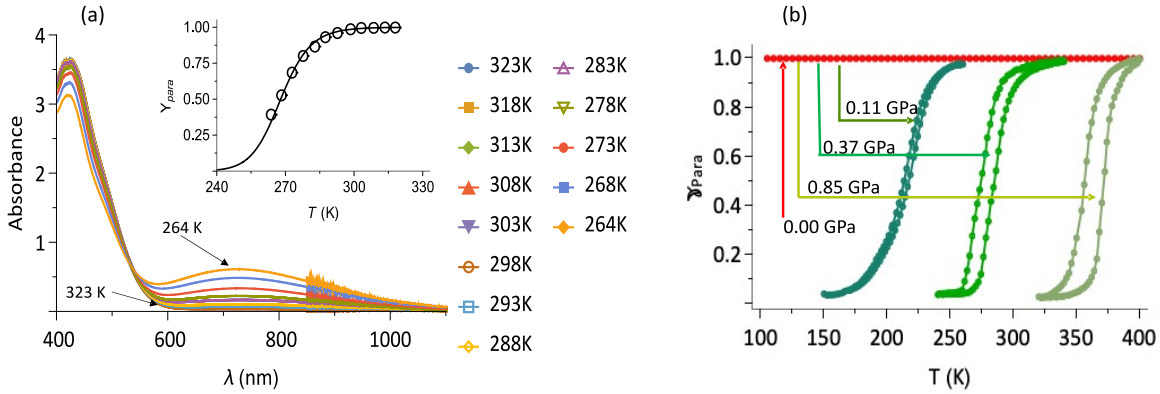

Fig. S6. (a) Variable temperature UV-Vis absorbance at 742 nm (maximum of the Fe^{II}-CN-Co^{III} IVCT band) of **1** in solution of MeOH at ambient pressure.[S1] The insert illustrates the molar fraction of paramagnetic species versus temperature derived from the UV-visible spectra. (b) Thermal ETCST of **1** in solid state under different hydrostatic pressures.[S2]

References

S1. S. De, J.-R. Jimenez, Y. Li, L.-M. Chamoreau, A. Flambard, Y. Journaux, A. Bousseksou and R. Lescouezec, *RSC Adv.*, 2016, 6, 17456–17459.

S2. Y. Li, A. Benchohra, B. Xu, B. Baptiste, K. Béneut, P. Parisiades, L. Delbes, A. Soyer, K. Boukheddaden and R. Lescouëzec, *Angewandte Chemie*, 2020, 132, 17425–17429.

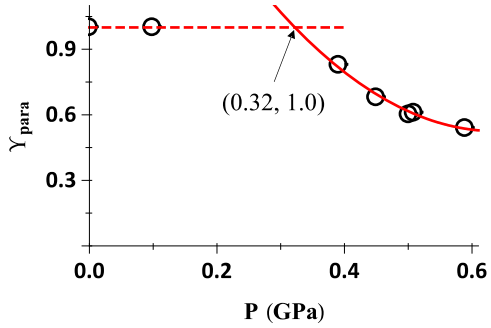

Fig. S7. Estimation of the pressure threshold (p_0 = 0.32 GPa) for para-dia conversion of **3**. γ_{para} = 1 for p < 0.32 GPa, γ_{para} = 2.461 – 6.064 P + 4.748 P^2 for p > 0.32 GPa.

V. HP-SC-XRD of 3 at 300 K

V-1. Phase transition provided by HP-SC-XRD

Table S4. Crystal data and structural refinement for the crystals SC1 and SC2 of **3** under increasing and decreasing pressure respectively.

Pressure (GPa)	**0.62(13)**	**0.76(2)**	**1.55(25)**	**1.77(2)**	**1.60(5)**	**1.15(2)**	**0.96(2)**	**0.71(2)**	**0.43(2)**	**0.11(6)**	**0.05(2)**
$P_{initial}$ (GPa)	0.5	0.75	1.3	1.78	1.55	1.15	0.95	0.72	0.45	0.17	0.05
P_{fin} (GPa)	0.75	0.78	1.8	1.76	1.65	1.15	0.97	0.7	0.45	0.05	0.05
Crystal	SC1 (increasing *p*)				SC2 (decreasing *p*)						
Space group	Triclinic, P-1				Triclinic, P-1						
a (Å)	13.437(8)	13.381 (12)	14.46(2)	14.22(4)	14.38(3)	14.24(3)	13.096(19)	13.206(19)	13.609(15)	13.633(19)	14.09(2)
b (Å)	13.901(5)	13.838 (8)	14.596(17)	14.43(4)	14.482(17)	14.582(17)	13.49(3)	13.72(3)	14.05(2)	14.05(3)	14.44(3)
c (Å)	14.296(5)	14.288 (8)	18.31(3)	17.74(5)	17.85(3)	18.16(3)	13.85(4)	13.95(3)	14.45(2)	14.35(3)	14.72(3)
α(°)	114.189(7)	114.146(12)	93.40(6)	92.59(12)	92.31(5)	93.15(7)	113.51(8)	114.15(6)	114.38(5)	114.29(6)	115.16(6)
β(°)	97.054(16)	97.12(2)	89.78(7)	91.10(15)	90.93(8)	90.84(8)	97.42(7)	96.32(7)	96.80(5)	96.60(6)	95.10(8)
γ(°)	115.907(15)	115.89(2)	91.68(6)	89.95(12)	90.72(6)	89.72(9)	115.81(6)	116.40(6)	115.85(4)	116.05(6)	116.90(7)
Z'	0,5	0,5	1	1	1	1	0,5	0,5	0,5	0,5	0,5
Volume ($Å^3$)	2037.3(17)	2019(2)	3855.(15)	3630.(30)	3713.(17)	3763.(17)	1879.(7)	1930.(9)	2109.(5)	2099.(6)	2266.(7)
V/Z'	4074.6	4038	3855	3630	3713	3763	3758	3860	4218	4198	4532
Struct. Solved	Yes	Yes	No	No	No	No	Yes	Yes	Yes	Yes	Yes
Independ. Refl.	8156, 2065	13002, 2056	29089	3282	30043	27019	7987, 2027	6342, 1956	11803,2166	8837, 2375	12004,2146
R_{int} (%)	10.88	15.08	0.221	13.7	0.3864	28.3	20.15	19.32	21.13	22.01	23.67
Structure solved	YES	YES	No	No	No	No	YES	YES	YES	YES	YES
Completeness	0.288	0.282	0.227	0.199	0.326	0.22	0.298	0.28	0.285	0.312	0.263
Dmin(Å), I/Sig	0.84, 7.2	0.83, 6.8	0.84, 2.4	0.80, 2.3	0.89, 2.5	0.84, 1.5	0.83, 3.9	0.83, 3.7	0.83, 4.3	0.83, 3.0	0.84, 4.4
R1, *wR2* (%)	7.83, 22.89	8.45, 23.80	-	-	-	-	10.38, 34.20	11.74, 37.59	10.57,34.46	12.87, 41.24	11.93, 38.70
Data/ param.	6.73	6.70	-	-	-	-	7.74	7.47	8.26	9.06	8.19
CCDC n°	2353837	2353844					2355116	2355117	2355118	2355119	2355120

As described in main text, we carried out high pressure XRD on two single crystals labelled SC1 and SC2. As the crystal quality decrease rapidly with time, we adopt therefore a strategy to measure quickly the crystal without waiting for the pressure stabilization. We collected data with increasing pressure for crystal SC1 and with decreasing pressure for crystal SC2. On the crystal SC1 we detected a phase transition (Figure 3) showing a doubling of the lattice volume between 0.76(2) GPa and 1.55(25) GPa.

It has not been possible to determine the high-pressure structure due to poor data quality. We therefore carried out experiment with SC2 by decreasing the pressure, unfortunately it was not possible to determine the high-pressure structure. However it show that the transition is reversible because by lowering the pressure we were able to recover the low pressure phase and it allow us to better identify the pressure range at which the transition takes place, between 1.15(5) GPa and

0.96(2)GPa. Moreover at 1.15(5) GPa we also detect some peak doubling (figure S8) which can be a clue for an ongoing phase transition. The R_{int} parameter indicates that data quality on SC2 is lower than on SC1 because of time decay of the crystal and also because of the measurements of the low- pressure phase after two transitions. Sometimes even if it was possible to solve the structure and show that the phase transition is reversible we have to constrain more the structure by refining only isotropic thermal motion parameters and by constraining some distances (C-N for 0.05GPa, and PF6 to be rigid, see the cif files deposit: CCDC n° 2355116-2355120). Moreover, the volume evolution is not reliable because at 0.11GPa the sample has to be re-centred during the experiment, introducing a possible bias in the volume estimation. The volume increase under pressure is an artefact due to the bad data).

Even the crystal structure of the high-pressure phase was not solved, the crystal transition is unambiguous as shown by the figure 3 where new diffraction peaks can be identified at high pressure. Moreover, as noted in main text, the low-pressure structure can be expressed in a non-conventional triclinic setting I-1 with cell parameters close to high pressure lattice. Despite significant changes in the parameters and angles between the two P-1 space group, the phase transition may result in a slight reorganization of the molecules in the crystal packing inducing a loss of the centering vector (see table 3 in the main text).

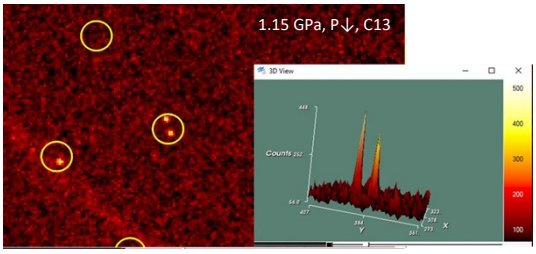

Figure S8. Peak doubling in the diffraction pattern of SC2 at 1.15 GPa.

V-2. Pressure-induced modification of the structures and intermolecular interactions of **3**

Table S5. Selected structural parameters for **3** (SC1) under pressure

Structural parameters	**P (GPa)**	**0.62 (300 K)**	**0.76 (300 K)**
Average	Fe-(CN)bridging	1.94 (3.5)	1.94 (3.5)
M-L	Fe-N(Tp)	1.97 (3.3)	1.97 (3.3)
Length* (Å)	Co-(NC)bridging	2.11 (2.5)	2.11 (2.5)
	Co-N(vbik)	2.11 (3)	2.11 (4.3)
	∑Fe	37.0	30.0
	∑Co	45.0	41.0
Different	∠N1C1-Fe	172 (3)	169 (4)
Angles (°)	∠N2C2-Fe	172 (3)	178 (4)
	∠C1N1-Co	162 (3)	164 (3)
	∠C2N2-Co	158 (3)	151 (3)
	Apex angle N-Co-N	95 (1)	93 (1)
	Apex angle C-Fe-C	84 (2)	86 (2)
	∠Co-C16=O1	170.3	172.0
vbik (°)	∠Co-C27=O2	173.2	173.1
	Dihedral angle vbik1	11.2	10.4
	Dihedral angle vbik2	13.6	12.2
Side and	d1[Fe···Co]	5.06	5.05
diagonal	d2[Fe···Co]	5.03	5.02
distances	diag[Fe···Fe]	7.40	7.38
(Å)	diag[Co···Co]	6.85	6.83

*The σ value for the average M-L length was calculated by averaging the σ values of each individual M-L length.

Table S6. Selected structural parameters for **3** (SC2) under different pressures at 300K compared to that obtained on a single crystal without DAC at 200K.

Structural parameters	**P (GPa)**	**0 (200 K)**	**0.05 (300 K)**	**0.11 (300 K)**	**0. 45 (300 K)**	**0.70 (300 K)**	**0.95 (300 K)**
Average	Fe-$(CN)_{bridging}$	1.918 (2.5)	1.90 (3.5)	1.91 (3.5)	1.94 (3)	1.82(4)	1.84(3)
M-L	Fe-N_{Tp}	1.975 (2.7)	1.93(4)	1.92(4)	1.96 (4)	1.87 (4)	1.94(4)
Length* (Å)	Co-$(NC)_{bridging}$	2.112 (2.5)	2.19 (3.5)	2.18(3.5)	2.13 (3)	2.12(3.5)	2.10(3.5)
	Co-N_{vbik}	2.137 (2.3)	2.11 (3)	2.11(3.5)	2.14 (3)	2.12(4.0)	2.10(3)
	∑Fe	23.00	30	27	38	38	25
	∑Co	38.06	52	48	38	39	39
Different	∠N1C1-Fe	172.2 (3)	177 (4)	176 (4)	173(3)	173 (4)	167 (4)
Angles (°)	∠N2C2-Fe	176.5 (3)	176 (3)	179 (4)	176(3)	175 (4)	176 (3)
	∠C1N1-Co	167.1 (2)	160 (4)	161 (4)	163(3)	160 (4)	164 (3)
	∠C2N2-Co	159.3 (2)	160 (3)	155 (3)	153(2)	149 (3)	148 (3)
	Apex angle N-Co-N	93.7 (1)	94 (1)	94 (1)	92 (1)	94 (1)	94 (1)
	Apex angle C-Fe-C	85.6 (1)	86 (2)	87 (2)	86 (1)	87 (2)	88 (2)
	∠Co-C16=O1	175.4	171.0	174.2	175.9	176.6	178.7
vbik (°)	∠Co-C27=O2	174.0	174.9	172.9	174.6	170.3	174.0
	Dihedral angle vbik1	8.83	9.6	11.8	8.3	11.4	11.1
	Dihedral angle vbik2	11.69	8.2	10.5	11.2	13.8	14.1
Side and	d1[Fe···Co]	5.11	5.16	5.08	5.11	4.95	4.95
diagonal	d2[Fe···Co]	5.08	5.11	5.04	5.06	4.96	4.93
distances	diag[Fe···Fe]	7.47	7.47	7.41	7.47	7.29	7.27
(Å)	diag[Co···Co]	6.93	7.05	6.89	6.91	6.70	6.69

*The σ value for the average M-L length was calculated by averaging the σ values of each individual M-L length.

The linear regression equations of M-L versus p data:

2.16 -0.071 p for Co-N_{bridge}

1.92 -0.047 p for Fe-C_{bridge}

2.12 - 0.016 p for Co-N_{vbik}

1.95 -0.009 p for Fe-N_{Tp}

The linear regression equations for the two Co-NC angles:

162.68 -0.091 p for ∠CoN1C1

158.96 – 10.56 p for ∠CoN2C2

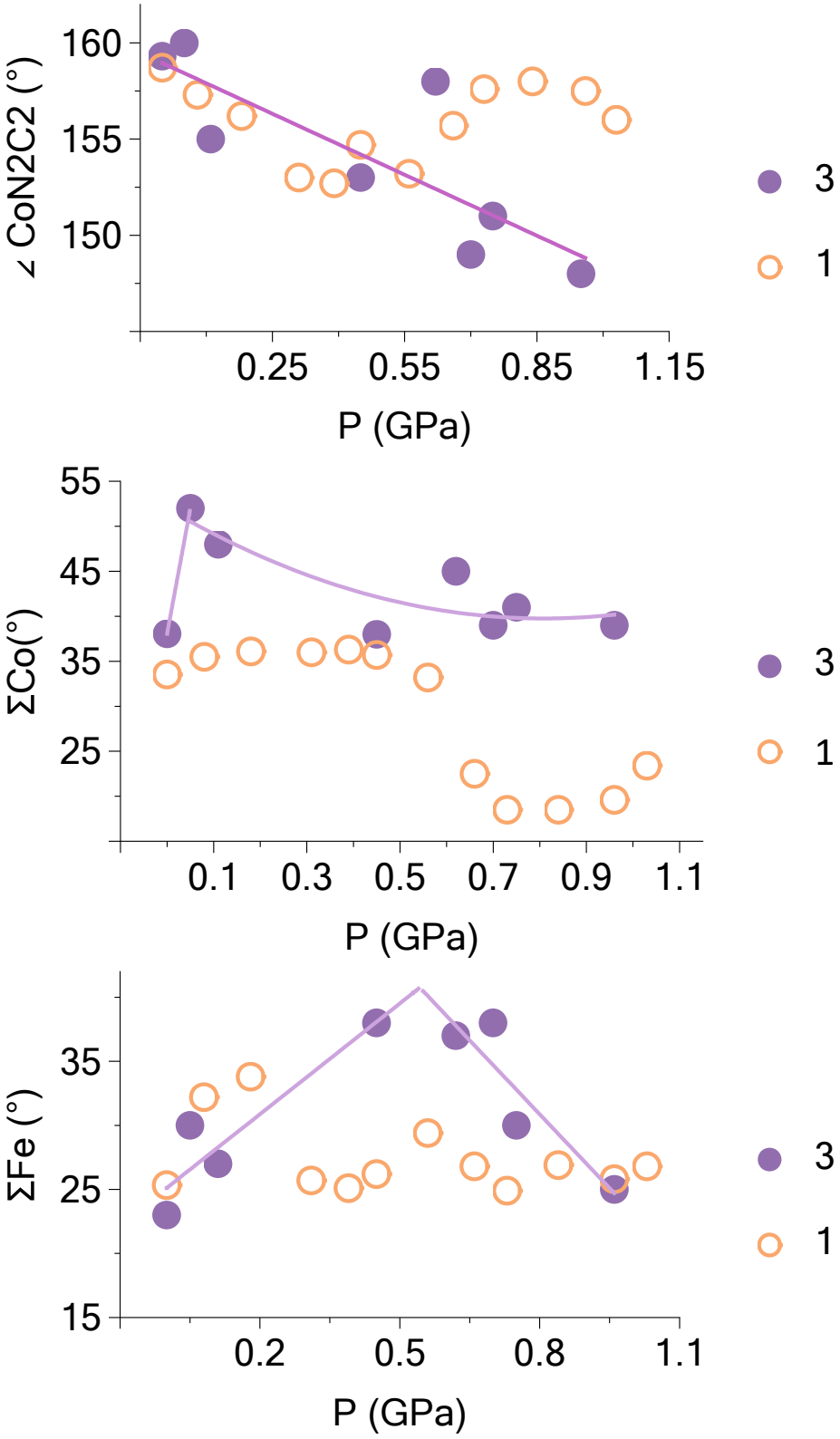

Fig. S9 Three distortion parameters versus pressure for the core structure of **3** and **1**: ∠CoN2C2 (above), ΣCo (middle) and ΣFe (bottom) The solid lines are for eye – guides.

VI. HP-Raman spectres of 3 under pressure at 200 K

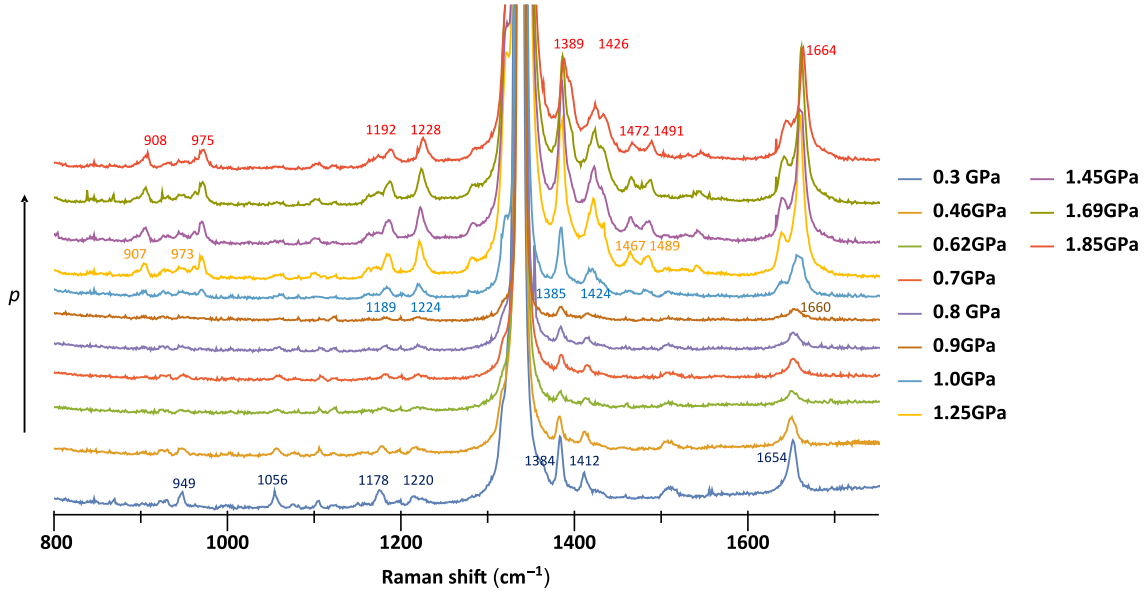

Figure S10. HP-Raman Spectra of **3** from 800 to 1750 cm^{-1} at 200 K with increasing pressure (0.30 – 1.85 GPa).

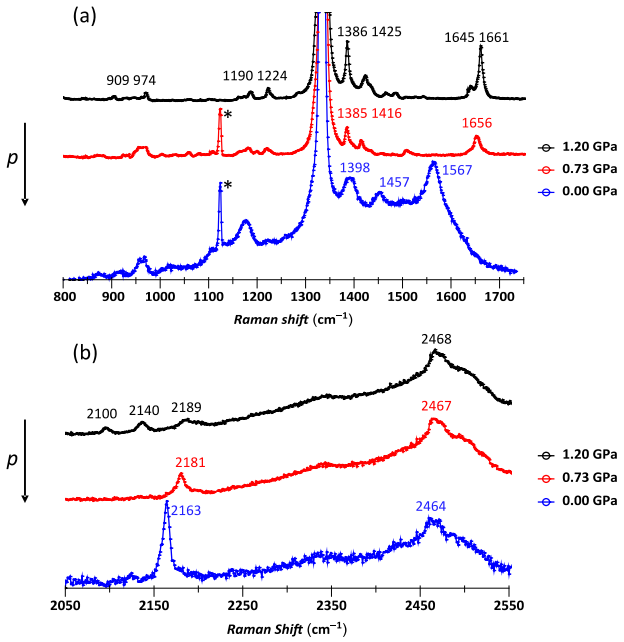

Figure S11. HP-Raman Spectra of **3** at 200 K with decreasing (1.20-0.0 GPa) pressure, from 800 to 1750 cm^{-1} (a) and from 2050 to 2550 cm^{-1} (b).

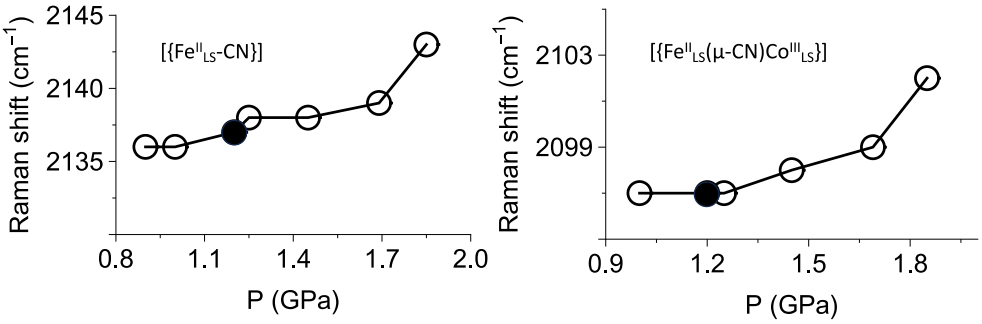

Figure S12. Blue shifts of Raman bands atributed to the vibration of the free [Fe^{II}-CN] group (left) and to that of [Fe^{II}-CN-Co^{III}] moiety (right). The circles represent the experimental data with increasing pressure and the disk, that with decreasing pressure.